Journal of Operation and Automation in Power Engineering
Vol. 7, No. 1, May 2019, Pages: 65 - 77
http://joape.uma.ac.ir

Adaptive Sliding Mode Control of a Multi-DG, Multi-Bus Grid-Connected Microgrid.

*F. Shavakhi Zavareh [1], E. Rokrok [1, *], J. Soltani [2, 3], M.R. Shakarami[1]*

[1] *Department of Technical & Engineering, Lorestan University, Khorramabad, Iran.*
[2] *Department of Electrical Engineering, Khomeinishahr Branch, Islamic Azad University, Isfahan, Iran.*
[3] *Faculty of Electrical and Computer Engineering, Isfahan University of Technology.*

Abstract- *This paper proposes a new adaptive controller for the robust control of a grid-connected multi-DG microgrid (MG) with the main aim of output active power and reactive power regulation as well as busbar voltage regulation of DGs. In addition, this paper proposes a simple systematic method for the dynamic analysis including the shunt and series faults that are assumed to occur in the MG. The presented approach is based on the application of the slowly time-variant or quasi-steady-state sequence networks of the MG. At each time step, the connections among the MG and DGs are shown by injecting positive and negative current sources obtained by controlling the DGs upon the sliding mode control in the normal and abnormal operating conditions of the MG. Performance of the proposed adaptive sliding mode controller (ASMC) is compared to that of a proportional-integral (PI)-based power controller and SMC current controller. The validation and effectiveness of the presented method are supported by simulation results in MATLAB-Simulink.*

Keyword: Adaptive sliding mode control, Dynamic analysis, Distributed generation, Microgrid, Unsymmetrical. Fault.

1. INTRODUCTION

A microgrid (MG) consists of a group of loads and distributed energy resources (DERs), such as distributed generations (DGs), battery energy storage systems (BESSs), photovoltaic cells, diesel engines, wind energy conversion systems, and fuel cells. An MG has the ability to operate grid-connected and islanded modes and manage the transitions between these two modes [1-2]. In the grid-connected mode, the main grid can provide the power shortage of the MG, and the additional power generated in the MG can be exchanged with the main grid. In the islanded mode, the real and reactive power generated by DGs should be in balance with the demand for local loads in Ref. [3]. Recently, MG analysis has become important due to the expansion of the MG system and automation of its operation. There are , however, certain operational challenges in the design of MG control and protection systems such as reliability assessment, energy management system, stability issues, and power quality. One of the characteristics of smart grids is uncertain generation and load profiles which have to be considered in evaluating the reliability of the MGs. In Ref. [4], the normal distribution function is used for representing uncertainties involved in both DG units and load demand within an MG. Moreover, in Ref. [5] employs an incentive-based demand response program and examines its effects on the MG energy management system problem. The objective functions of the MG energy management system problem include total cost and emission. The main control variables for the MG control are voltage, frequency, and active and reactive power; in the grid-connected mode, the frequency and the voltage at the PCC are dominantly determined by the main grid in Ref. [3]. With respect to the control of DGs and the analysis of inverter-based MGs under unbalanced load and external fault conditions, the employment of appropriate power, current, and voltage control strategies is very important for enhancing power quality [6-10]. Some possible control strategies that distributed power generation systems can use under grid disturbances in the MG are discussed in Ref. [6]. This paper provides strategies for generating current references, and analytical equations are provided and discussed.

Received: 28 May. 2018
Revised: 17 Agust 2018 and 10 October 2018
Accepted: 00 Mar. 00
*Corresponding author:
E-mail: rokrok.e@lu.ac.ir (E. Rokrok)
Digital object identifier: 10.22098/joape.2019.4843.1371
Research Paper

However, the elimination of active and reactive power oscillations is obtained only by accepting highly distorted currents. In Ref. [7], a flexible voltage support control scheme has been proposed for three-phase DG inverters under a grid fault. A control algorithm was presented for the reference current generation, providing flexible voltage support under grid faults. However, a voltage support control loop should be developed and active and reactive power oscillations should be eliminated. A control strategy is proposed in Ref. [8] to obtain the control of power and current quality without requiring a positive/negative-sequence extraction calculation. Nevertheless, in this paper, a PR controller is utilized for current regulation whose resonant frequency should be updated with the grid frequency for operating the PR controller under grid fault. Furthermore, a control strategy is proposed in Ref. [9] to obtain the flexible power control and successful fault ride through (FRT) within a safe current operation range under grid faults. However, with the proposed method, the peak current can be controlled within the rated value only by accepting the highly unbalanced currents and voltages. In addition, a multivariable controller is presented in Ref. [10] for power electronic-based DER units. The method includes a multiple-input and multiple-output (MIMO) repetitive controller for sinusoidal disturbance rejection. The control strategy proposed in Ref. [10] is specifically designed to mitigate the effect of Adaptive sliding mode control (ASMC) is a powerful and effective control technique with the capability of the access to desired responses in the presence of uncertainties and external disturbances. The important characteristics of ASMC are robustness to parametric uncertainties, quick responses, computational simplicity, and excellent transient performance. [11-13]. The combination of adaptive control techniques and SMC is established as a beneficial robust technique for MG control with real external disturbances and parametric uncertainties [14-18]. In Ref. [14], an adaptive sliding-mode controller is proposed for the rejection of external disturbances and internal perturbation so as to guarantee the globe robustness of the control system of the inverter in the islanded MG. However, only the output voltage of the DG system is controlled, while no control is exercised over the output current. A voltage-control strategy for an inverter-based DG system in the islanded MG is presented in Ref. [15]; based on fractional-order SMC. Nevertheless, the fractional-order SMC proposed in Ref. [15] controls the terminal voltage of the DG system, with no control on the VSC AC-side current. In the control scheme proposed in Ref. [16], SMC strategy is employed for distributed energy resource (DER) units in the islanded MG. The proposed control strategy provides a fast and stable control of the terminal voltage and frequency of DG. However, the negative components of voltage and current are not discussed in the control scheme in Ref. [16]. A recursive fast terminal sliding mode control (FTSMC) is presented in Ref. [17] for an MG system operating in grid-connected and islanded mode of operation. The recursive approach of FTSMC is utilized in the voltage source inverter to control the bus voltage nearer to the main grid and farther away from the micro-source in a grid-connected system. Furthermore, in Ref. [18] proposes a robust control strategy for a grid-connected MG that employs an adaptive Lyapunov function-based control scheme to directly compensate for the negative-sequence current components, and a sliding mode-based control scheme to directly regulate the positive-sequence active and reactive power injected by DG units to the MG. This adaptive SMC, however, controls the terminal positive sequence of active power and negative sequence of the current of the DG system, with no control over the voltages.

Some analytical models exist for distribution systems under unbalanced and fault conditions, including EMTP which is quite detailed and is used to analyze fast electromagnetic transients [19-20]. Simulation of the complete power system with EMTP is computationally inefficient since too small simulation step sizes are employed for the calculation of fast electromagnetic transients and EMTP requires extensive computational effort when a complex system is simulated. Other models are based on the dynamic phasors (DP) technique and complex Fourier coefficients [21-23]. In most of these papers, only DGs and loads are modeled based on dynamic phasors and the network is based on quasi-stationary models. The major disadvantage of the aforementioned analytical models for large-scale systems is the complexity and increased number of state equations which in turn cause a high computational burden. To study different faults, no systematic method has been presented and, so far, only few complicated equations have been developed for this purpose which are troublesome and storage- and time-consuming.

In all the aforementioned methods, only the output voltage or current or the power of the DG is controlled, whereas no control is exerted over all of them. The main contribution of the present paper is to propose a control structure based on adaptive sliding mode control for fast and stable regulation of the output of active and reactive power and voltage of DG units. Two adaptive sliding mode controllers are designed in order to regulate the positive- and negative-sequence active and reactive

power injected by DG units to the MG under balanced and unbalanced conditions during normal and fault conditions. Moreover, this paper presents an unsymmetrical fault analysis method based on quasi-stationary time-varying phasors in the multi-DG MG. In each step of time, the connections between the DGs and MG are shown by injecting time-variant space phasor currents obtained by the sliding mode control of DGs under normal and fault conditions. The adaptive sliding mode control method is used to (1) regulate the output active power and voltage of the DGs in the normal mode, and (2) eliminate the negative-sequence output voltage and regulate the output active powers and positive-sequence voltage of DGs in unbalanced and fault conditions.

The content of this paper is organized as follows: The first section describes the main concept of slow and fast time-variant space phasors in a synchronous reference frame attached to the main grid. In Section III, the proposed method for dynamical modeling of the MG under fault conditions is presented. In Section IV, the developed adaptive sliding mode control is extended to be used for DG control under MG faulted conditions. Simulations are performed in Section V to verify the validity and effectiveness of the proposed control methods. Finally, conclusions are given in Section VI.

2. CONCEPT OF SLOWLY AND FAST TIME VARIANT SPACE PHASOR

Assuming a transmission line connected between busbars m and n in a typical MG as shown in Fig. (1-a), the instantaneous voltage equation of this line in the abc reference frame is given by:

$$v_{abc,m}(t) - v_{abc,n}(t) = v_{abc,l}(t) = Ri_{abc}(t) + L\frac{di_{abc}(t)}{dt} \quad (1)$$

(a)

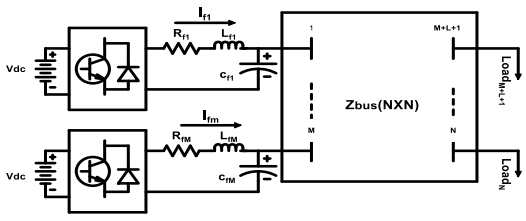

(b)

Fig.1. a) Representation of a typical transmission line, b) multi-bus multi-DG MG

Transferring Eq. 1 to the dq synchronous reference frame leads to:

$$V_{dql}^{e}(t) = RV_{dq}^{e}(t) + L\frac{dV_{dql}^{e}}{dt} \mp \omega_s LV_{qd}^{e}(t) \quad (2)$$

where, ω_s is the synchronous angular speed and $V_{dql}^{e}(t)$and $V_{dq}^{e}(t)$ are the fast time-variant space phasors which define the time-varying phasors as:

$$\bar{V}_l(t) = V_{dl}^{e}(t) + jV_{ql}^{e}(t), \bar{I}_l(t) = I_{dl}^{e}(t) + jI_{ql}^{e}(t) \quad (3)$$

Considering (2), (3) it can be obtained that

$$\bar{V}_l(t) = R\bar{I}_l(t) + j\omega_s L\bar{I}_l(t) + L\frac{d\bar{I}_l(t)}{dt} \quad (4)$$

where; $\bar{V}_l(t)$ and $\bar{I}_l(t)$ are the fast time-variant voltage and current space phasors which describe high-frequency effects. By ignoring the time derivative terms in Eq. 4 (which is the transient DC currents of the transmission line), the slowly or quasi-state time-variant space phasors are obtained as:

$$V_l(t) = RI_l(t) + j\omega_s LI_l(t) \quad (5)$$

where, $V_l(t)$ and $I_l(t)$ are the slowly time-variant voltage and current space phasors. In fact, the quasi-state time-variant assumption amounts to neglecting $\frac{d\bar{I}_l(t)}{dt}$ term in Eq. (4). By combining models of elementary passive components, any symmetric transmission network can be modeled based on the *dq* reference frame. The traditional quasi-static model is based on the assumption that the frequency of voltage and current signals throughout the network is approximately constant. As a result, AC signals can be modeled accurately enough by means of time-varying phasors, and the transmission network can be described by the constant admittance matrix *Y* through the following linear relation [24]:

$$I(t) = YV(t) \quad (6)$$

where Y is the admittance matrix of the n-bus network. This is a quasi-static model of the transmission network, since it is based on the assumption that phasors change slowly in comparison to ω_s. Based on this assumption, the frequency is approximately constant throughout the network and, as a result, matrix Y_{bus} is composed of constant admittances which are computed at fixed frequency ω_s [24]. Extensive demonstration of Eq. 6 in terms of d-q components of the voltage of the grid nodes and the pure injectable currents can be expressed as Eq. 7. where g_{ij} and b_{ij} represent the real and imaginary part of y_{ij} from Y bus admittance matrix of the network. Direct comparison of these equations reveals that both models are similar, except for the additional time derivative terms in the dq0 model which describe high-frequency effects. Note that, at low frequencies, where the time derivatives are negligible, the two models are equivalent in Ref. [25].

$$\begin{bmatrix} I_{1d} \\ I_{1q} \\ . \\ . \\ . \\ I_{nd} \\ I_{nq} \end{bmatrix} = \begin{bmatrix} \begin{bmatrix} g_{11} & -b_{11} \\ b_{11} & g_{11} \end{bmatrix} \begin{bmatrix} g_{12} & -b_{12} \\ b_{12} & g_{12} \end{bmatrix} \cdots \begin{bmatrix} g_{1n} & -b_{1n} \\ b_{1n} & g_{1n} \end{bmatrix} \\ . \quad . \quad . \quad . \quad . \\ . \quad . \quad . \quad . \quad . \\ . \quad . \quad . \quad . \quad . \\ \begin{bmatrix} g_{n1} & -b_{n1} \\ b_{n1} & g_{n1} \end{bmatrix} \begin{bmatrix} g_{n2} & -b_{n2} \\ b_{n2} & g_{n2} \end{bmatrix} \cdots \begin{bmatrix} g_{nn} & -b_{nn} \\ b_{nn} & g_{nn} \end{bmatrix} \end{bmatrix} \begin{bmatrix} V_{1d} \\ V_{1q} \\ . \\ . \\ . \\ V_{nd} \\ V_{nq} \end{bmatrix} \quad (7)$$

3. DYNAMIC FAULTS ANALYSIS OF THE MICROGRID

3.1. Shunt Faults

It is well-known that, under unsymmetrical fault conditions system voltages and currents can be written in terms of different sequence (positive, negative, and zero) components [20]. Under unsymmetrical faults, the DG currents and voltages can be decomposed into components due to positive-, negative-, and zero-sequence components:

$$I(t) = YV(t), \quad I = I^+ + I^- + I^0, \; V = V^+ + V^- + V^0 \quad (8)$$

Then, the connection between the DGs and MG can be demonstrated by injecting the DG currents' positive-, negative-, and zero-sequence components. Considering an arbitrary shunt or series fault occurring at a certain point (P) located in the MG network (Fig. (2)), the conventional approach described in the power system textbooks for shunt and series faults in the sinusoidal steady-state conditions can be extended for the dynamic analysis of these faults based on slowly fast time-variant space phasors of networks as described here.

The Thévenin equivalent circuits corresponding to the networks depicted in Fig. (2) can be obtained as shown in Fig. (3). Using Fig. (3), the configuration of shunt faults can be obtained as described in Table I [26]. Let us consider a fictitious bus at the fault location in each sequence network. In Fig. (3), Z_{PP}^{+}, Z_{PP}^{-} and Z_{PP}^{0} are the deriving positive-, negative-, and zero-sequence impedances corresponding to virtual bus (P) where the fault occurs. Furthermore, E_{th}^{+} and E_{th}^{-} are the Thévenin open-circuit voltages given by

$$E_{th}^{+} = \sum_{i=1}^{M} Z_{iP} I_i^{+}(t) + \sum_{j=1}^{L} Z_{jP} I_{lj}^{+}(t), \quad E_{th}^{-} = \sum_{i=1}^{M} Z_{iP} I_i^{-}(t) + \sum_{j=1}^{L} Z_{jP} I_{lj}^{-}(t) \quad (9)$$

where; I_i is the space current phasor injected by the i^{th} DG to bus-bar (i) and I_{lj} is the space current phasor injected by the j^{th} load. For each arbitrary shunt fault, the Thévenin equivalent circuits are combined on the basis of the information given in Table 1.

For an arbitrary shunt fault occurring in the MG, the connections between MG networks' sequences are shown in Table I based on the application of slowly time-variant space phasors. For a given shunt fault, by using Thévenin equivalent circuits (Fig. (3)) and the information given in Table I, the positive and negative sequences' fault currents defined by (I_p^{+}) and (I_p^{-}) are obtained and injected at fault points (P^{+}) and (P^{-}), respectively (Fig. (2)). These currents in combination with the DGs' injected currents are used to obtain the positive and negative busbar voltages corresponding to these DGs in the subsequent time step (Δt).

3.2. Series Faults

Series faults can occur along the power lines as the result of an unbalanced series impedance condition of the lines in the case of one or two broken lines. In practice, a series fault is encountered, for example, when lines (or circuits) are controlled by circuit breakers (or fuses) or any device that does not open all three phases; one or two phases of the line (or the circuit) may be open, while the other phase(s) is closed. The present paper focuses on single- and two-conductor breaking faults. Similar to the shunt faults, the Thévenin equivalent circuits of Fig. (4) are given in Fig. (5). Using these equivalent circuits and the data in Table 2, these two types of series faults can be studied with the same procedure described for the shunt faults in the previous section.

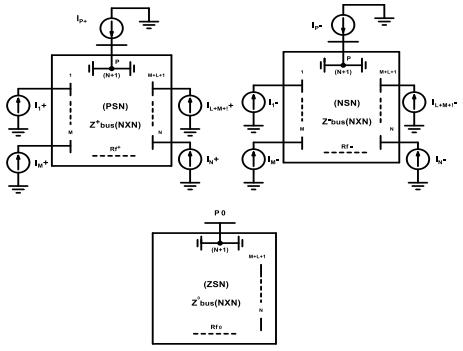

Fig. 2. Positive, negative, and zero sequence networks corresponding to shunt faults.

Referring to [26], the connections between power sequences' networks corresponding to a given series fault are given Table 2.

Referring to Ref. [26], the equivalent Thévenin circuits corresponding to Fig. (4) can be represented by the following circuits. Assuming a type of series faults (one-open-conductor or two-open-conductor) as shown in Table 2, and using the Thévenin equivalent circuits shown in Fig. (5), the positive and negative fault points

$((I_{P1}^{+}(t), I_{P2}^{+}(t))$ and $((I_{P1}^{-}(t), I_{P2}^{-}(t))$ are obtained and injected into fault points $((P_1^{+}, P_2^{+})$ and (P_1^{-}, P_2^{-}), respectively. Based on Fig. (4), these currents in $((I_{P1}^{+}(t), I_{P2}^{+}(t))$ and $((I_{P1}^{-}(t), I_{P2}^{-}(t))$ are obtained and injected into fault points $((P_1^{+}, P_2^{+})$ and (P_1^{-}, P_2^{-}), respectively. Based on Fig. (4), these currents in combination with the DGs injected currents are employed to obtain the positive and negative busbar voltages in the subsequent time step(Δt).

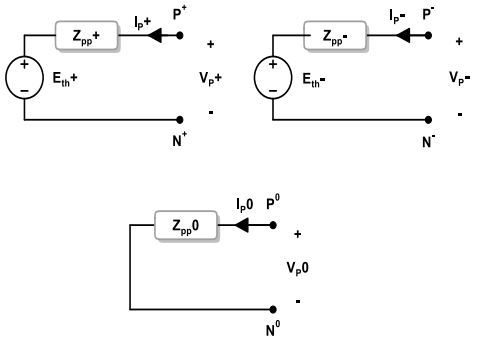

Fig. 3. Positive, negative, and zero Thévenin equivalent circuits seen at the fault point (P).

Table I. Representation of sequence network connection for different shunt faults.

Fault Type	The Connection of Sequence Networks
Phase (a) to ground fault	$P^{+} \rightarrow N^{-}$, $P^{-} \rightarrow N^{0}$, $P^{0} \rightarrow N^{+}$
b-c short circuit fault	$P^{+} \rightarrow P^{-}$, $N^{+} \rightarrow N^{-}$
b-c-g fault	$P^{+} \rightarrow P^{-} \rightarrow P^{0}$, $N^{+} \rightarrow N^{-} \rightarrow N^{0}$
Three-phase short circuit fault	$P^{+} \rightarrow N^{+}$

($\rightarrow$: DENOTES the point connection)

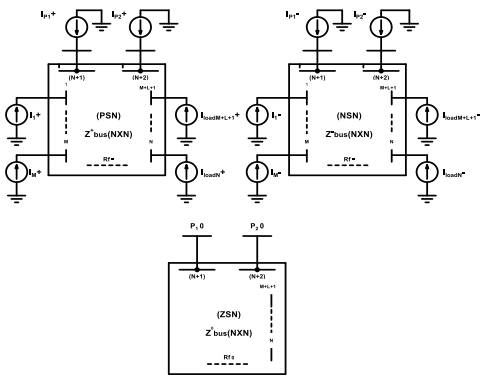

Fig. 4. Positive, negative, and zero sequence networks corresponding to series faults.

Table II. Sequence network connections for series fault

Conductor breaking	The connection of sequence networks
Breaking of the coductor (a)	$P_1^{+} \rightarrow P_1^{-}$, $P_2^{+} \rightarrow P_2^{-}$
Breaking of the coductors (b,c)	$P_2^{+} \rightarrow P_1^{-}$, $P_2^{-} \rightarrow P_1^{0}$, $P_2^{0} \rightarrow P_1^{+}$

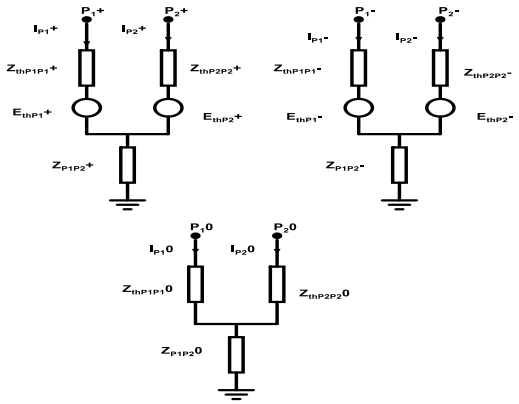

Fig. 5. The Thévenin equivalent circuit of Fig. 4.

4. DEVELOPING THE ADAPTIVE SLIDING MODE CONTROL

Considering the k^{th} inverter-based DG electrical circuit configuration as shown in Fig. (1-b), the DG unit is represented by a DC power supply, a VSC, and an LC-filter connected to the bus of V_{fk}. The system parameters are given in Table III. Using the well-known Park transformation and considering the parameters in the nominal condition, the current and voltage dynamics in the synchronous reference frame can be derived as:

$$\frac{di_{fdk}(t)}{dt} = \frac{1}{L_{fk}}(v_{idk}(t) - R_{fk}i_{fdk}(\mathrm{t}) - v_{fdk}(\mathrm{t})) + \omega_0(t)i_{fqk}(t) \quad (10)$$

$$\frac{di_{fqk}(t)}{dt} = \frac{1}{L_{fk}}(v_{iqk}(t) - R_{fk}i_{qk}(\mathrm{t}) - v_{fqk}(\mathrm{t})) - \omega_0(t)i_{fdk}(t) \quad (11)$$

$$\frac{dv_{fdk}(t)}{dt} = \frac{1}{C_{fk}}(i_{fdk}(\mathrm{t}) - i_{odk}(\mathrm{t})) + \omega_0(t)v_{fqk}(t) \quad (12)$$

$$\frac{dv_{fqk}(t)}{dt} = \frac{1}{C_{fk}}(i_{fqk}(\mathrm{t}) - i_{oqk}(\mathrm{t})) - \omega_0(t)v_{fdk}(t) \quad (13)$$

Considering the parameters in the nominal condition, Eqs. 10-13 can be rewritten as:

$$\frac{di_{fdk}(t)}{dt} = \alpha(v_{idk}(t) - \beta i_{fdk}(\mathrm{t}) - v_{fdk}(\mathrm{t})) + \omega_0(t)i_{fqk}(t) \quad (14)$$

$$\frac{di_{fqk}(t)}{dt} = \alpha(v_{iqk}(t) - \beta i_{qk}(\mathrm{t}) - v_{fqk}(\mathrm{t})) - \omega_0(t)i_{fdk}(t) \quad (15)$$

$$\frac{dv_{fdk}(t)}{dt} = \gamma(i_{fdk}(\mathrm{t}) - i_{odk}(\mathrm{t})) + \omega_0(t)v_{fqk}(t) \quad (16)$$

$$\frac{dv_{fqk}(t)}{dt} = \gamma(i_{fqk}(t) - i_{oqk}(t)) - \omega_0(t)v_{fdk}(t) \quad (17)$$

where $\alpha = \frac{1}{L_{fk}}, \beta = R_{fk}, \gamma = \frac{1}{C_{fk}}$ are the nominal parameter values. If the parameters of the system deviate from their nominal values, Eqs. 14-17 can be modified as:

$$\frac{di_{fdk}(t)}{dt} = \alpha(v_{idk}(t) - \beta i_{fdk}(t) - v_{fdk}(t)) + \omega_0(t)i_{fqk}(t) + \eta_d \quad (18)$$

$$\frac{di_{fqk}(t)}{dt} = \alpha(v_{iqk}(t) - \beta i_{qk}(t) - v_{fqk}(t)) - \omega_0(t)i_{fdk}(t) + \eta_q \quad (19)$$

$$\frac{dv_{fdk}(t)}{dt} = \gamma(i_{fdk}(t) - i_{odk}(t)) + \omega_0(t)v_{fqk}(t) + \vartheta_d \quad (20)$$

$$\frac{dv_{fqk}(t)}{dt} = \gamma(i_{fqk}(t) - i_{oqk}(t)) - \omega_0(t)v_{fdk}(t) + \vartheta_q \quad (21)$$

where η_{dq} and ϑ_{dq} are the lumped-sum uncertainties which can be written as:

$$\eta_{dq} = \Delta\alpha\left(v_{idqk}(t) - \beta i_{fdqk}(t) - v_{fdqk}(t)\right) - \Delta\beta(\alpha + \Delta\alpha)i_{fdqk}(t) + \delta_{dq}$$
$$\vartheta_{dq} = \Delta\gamma\left(i_{fdqk}(t) - i_{odqk}(t)\right) + \nu_{dq} \quad (22)$$

where Δ denotes a difference from the nominal value and the terms δ_{dq} and ν_{dq} are added to account for system dynamic disturbances and other un-modeled uncertainties.

It is assumed that the LC-filter and interlink-line have balanced three-phase impedance since each equation (10) to (13) can be fully decoupled into positive and negative sequences. Under the unbalanced condition, each voltage and current can be expressed as:

$$v_{fd} = v_{fd}^{+} + v_{fd}^{-}, v_{fq} = v_{fq}^{+} + v_{fq}^{-}$$
$$i_{fd} = i_{fd}^{+} + i_{fd}^{-}, i_{fq} = i_{fq}^{+} + i_{fq}^{-} \quad (23)$$

It must be noted that in the dq coordinate [20]:

1) Positive-sequence DG quantities appear as DC values; and

2) Negative-sequence DG quantities exhibit the second harmonics of fundamental frequency and are, therefore, time-variant.

Instantaneous active and reactive power injected by the DG unit to the MG can be represented as:

$$P_f = \frac{3}{2}(v_{fd}(t)i_{fd}(t) + v_{fq}(t)i_{fq}(t))$$
$$Q_f = \frac{3}{2}(v_{fq}(t)i_{fd}(t) - v_{fd}(t)i_{fq}(t)) \quad (24)$$

The proposed control structure consists of an adaptive sliding mode based on the positive and negative power controller on the reference values of ($P_f^{+,*}, v_f^{+,*}$) and ($P_f^{-,*} = 0, v_f^{-,*} = 0$). The positive power controller is designed to regulate the positive sequence of active and reactive power injected by the DG unit to the MG, whereas the negative power controller is designed to compensate for the impact of negative sequence voltage of the unbalanced loads and faulty conditions. At each time step Δt (in second), the output positive- and negative-sequence of currents' space phasor correspond to the DGs and loads ($\bar{Z}_{li}$) are injected to the positive- and negative-sequence networks of the MG, respectively (Fig. (6-a)).

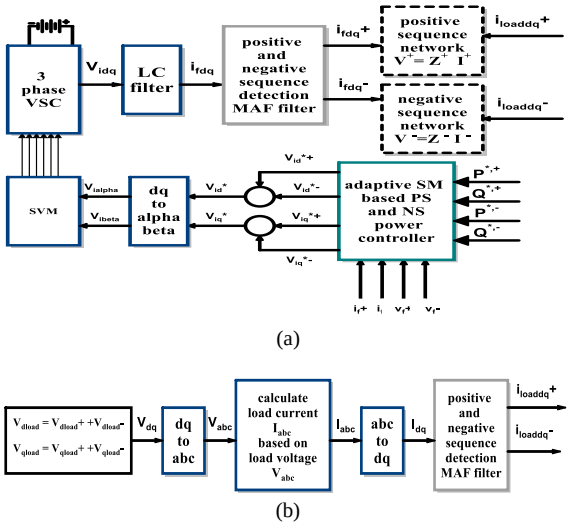

Fig6. a) Block diagram for the proposed fault analysis method; b) block diagram for calculating positive and negative unbalanced load currents.

Note that, for unbalanced loads of($\bar{Z}_{li}$), it is necessary to obtain the load current $\bar{I}_{abc}(t)$ first and then, according to the block diagram shown in Fig. (6-b), calculate the positive and negative sequences of load currents I_{loaddq}^{+} and I_{loaddq}^{-}. The main control objective for PQ controlled DG units is to regulate the active and reactive power injected by the DG unit to the MG. To enhance the transient response and provide desirable disturbance rejection and reference-tracking performance, an adaptive sliding mode controller based on the direct power control method is proposed for positive- and negative-sequence active and reactive power of all DG units. For this purpose, the integral based sliding surface is selected as [27]:

$$S = \begin{bmatrix} S_{Pf} \\ S_{Qf} \end{bmatrix},$$
$$S_{Pf} = e_{Pf} + K_{IP}\int_0^t e_{Pf}dt\,, \quad S_{Qf} = e_{Qf} + K_{IQ}\int_0^t e_{Qf}dt \quad (25)$$

where K_{IP} and K_{IQ} are positive constant gains ande_{Pf}, e_{Qf} are the error signals corresponding to the output active and reactive powers and voltage of the DG, given by:

$$e_{Pf} = P_f^* - P_f, \qquad e_{Qf} = Q_f^* - Q_f \tag{26}$$

where superscript (*) denotes to reference values. Reactive power reference (Q_f^*) is defined as:

$$Q_f^* = K_{Iv} \int_0^t e_{vf} dt \tag{27}$$

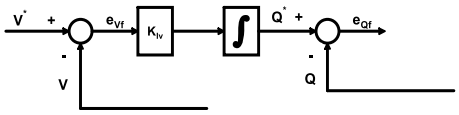

Fig. 7. Reactive power reference

Based on the sliding mode control, it is required to restrict the controlled state onto its corresponding sliding surfaces [30]. This is exclusively governed by:

$$\begin{bmatrix} S_{Pf} \\ S_{Qf} \end{bmatrix} = \frac{d}{dt}\begin{bmatrix} S_{Pf} \\ S_{Qf} \end{bmatrix} = 0 \tag{28}$$

Considering (28), differentiating (25) with respect to time gives:

$$\frac{d}{dt}S_{Pf} = \frac{d}{dt}e_{Pf} + K_{IP}e_{Pf} = -\frac{d}{dt}P_f + K_{IP}e_{Pf} = 0 \tag{29}$$

$$\frac{d}{dt}S_{Qf} = \frac{d}{dt}e_{Qf} + K_{IQ}e_{Qf} = -\frac{d}{dt}Q_f + K_{IQ}e_{Qf} = 0 \tag{30}$$

By substituting $\frac{d}{dt}\begin{bmatrix} P_f \\ Q_f \end{bmatrix}$ from (18-22) and (23-24) into (29-30) it can be shown that:

$$\frac{d}{dt}\begin{bmatrix} S_{Pf} \\ S_{Qf} \end{bmatrix} = -A\begin{bmatrix} i_{fd} \\ i_{fq} \end{bmatrix} - \begin{bmatrix} v_{fd} & v_{fq} \\ v_{fq} & -v_{fd} \end{bmatrix} B - \frac{3}{2}\begin{bmatrix} v_{fd} & v_{fq} \\ v_{fq} & -v_{fd} \end{bmatrix}\begin{bmatrix} \alpha v_{id} \\ \alpha v_{iq} \end{bmatrix} - \mu_s + \begin{bmatrix} K_{IP} & 0 \\ 0 & K_{IQ} \end{bmatrix}\begin{bmatrix} e_{Pf} \\ e_{Qf} \end{bmatrix} \tag{31}$$

Where

$$A = \frac{3}{2}\begin{bmatrix} \gamma(i_{fd} - i_{od}) + \omega_0 v_{fq} & \gamma(i_{fq} - i_{oq}) - \omega_0 v_{fd} \\ \gamma(i_{fq} - i_{oq}) - \omega_0 v_{fd} & -\gamma(i_{fd} - i_{od}) - \omega_0 v_{fq} \end{bmatrix} \tag{32}$$

$$B = \frac{3}{2}\begin{bmatrix} \alpha(-v_{fd} - \beta i_{fd}) + \omega_0 i_{fq} \\ \alpha(-v_{fq} - \beta i_{fq}) - \omega_0 i_{fd} \end{bmatrix}$$

$$\mu_s = \frac{3}{2}\begin{bmatrix} \eta_d & \eta_q \\ \eta_q & -\eta_d \end{bmatrix}\begin{bmatrix} i_{fd} \\ i_{fq} \end{bmatrix} + \frac{3}{2}\begin{bmatrix} v_{fd} & v_{fq} \\ v_{fq} & -v_{fd} \end{bmatrix}\begin{bmatrix} \vartheta_d \\ \vartheta_q \end{bmatrix} \tag{33}$$

If the control law is designed as:

$$u = u_{eq} + u_{sw}$$

$$u = \begin{bmatrix} v_{id} \\ v_{iq} \end{bmatrix} = \frac{2}{3\alpha}\begin{bmatrix} v_{fd} & v_{fq} \\ v_{fq} & -v_{fd} \end{bmatrix}^{-1}\left\{-A\begin{bmatrix} i_{fd} \\ i_{fq} \end{bmatrix} - \begin{bmatrix} v_{fd} & v_{fq} \\ v_{fq} & -v_{fd} \end{bmatrix} B + \begin{bmatrix} K_{IP} & 0 \\ 0 & K_{IQ} \end{bmatrix}\begin{bmatrix} e_{Pf} \\ e_{Qf} \end{bmatrix} + u_{sw}\right\} \tag{34}$$

where u_{eq} is used for the nominal system and u_{sw} is a new control input to be determined, $\frac{d}{dt}\begin{bmatrix} S_{Pf} \\ S_{Qf} \end{bmatrix}$ can be given by:

$$\frac{d}{dt}S = \frac{d}{dt}\begin{bmatrix} S_{Pf} \\ S_{Qf} \end{bmatrix} = -u_{sw} - \mu_s \tag{35}$$

Letting

$$\tilde{\mu}_s = \hat{\mu}_s - \mu_s \tag{36}$$

be the error between the lumped-sum uncertainties μ_s and its estimated value$\hat{\mu}_s$, a Lyapunov function can be defined as follows:

$$V = \frac{1}{2}S^T S + \frac{1}{2}\tilde{\mu}_s^T \gamma_s \tilde{\mu}_s \tag{37}$$

where γ_s is a diagonal matrix with all positive constant diagonal entries which are the adaptation law gains. Differentiating V with respect to time gives:

$$\frac{d}{dt}V = S^T\left(\frac{d}{dt}S\right) + \tilde{\mu}_s^T \gamma_s \left(\frac{d}{dt}\tilde{\mu}_s\right) \tag{38}$$

Considering (35), it can be concluded that:

$$\frac{d}{dt}V = S^T(-u_{sw} - \mu_s) + \tilde{\mu}_s^T \gamma_s \left(\frac{d}{dt}\tilde{\mu}_s\right) \tag{39}$$

If the adaptation law is chosen as:

$$\frac{d}{dt}\tilde{\mu}_s = -\gamma_s^{-1} S \tag{40}$$

then,

$$\frac{d}{dt}V = S^T(-u_{sw} - \hat{\mu}_s) \tag{41}$$

The magnitude of uncertainties must be bounded to keep the trajectory on the sliding surface. Thus, the positive constant diagonal matrix ρ is chosen to be larger than the magnitude of uncertainties

$$\rho > |\chi_s| \tag{42}$$

and the control input is selected as:

$$u_{sw} = -\hat{\mu}_s + K_s S + \rho sat(S) \tag{43}$$

where; K_s is a positive constant diagonal matrix and the saturation function $sat(.)$ is described by

$$sat(x) = \frac{x}{|x| + r} \tag{44}$$

where; r is a small positive constant gain and $r \ll |x|$. Since the selection of the upper bound of lumped uncertainty has a significant effect on control performance, the bound is estimated through an adaptive estimation technique:

$$\frac{d}{dt}\hat{\rho} = K_\rho |S| \tag{45}$$

where; K_ρ is a positive constant diagonal matrix. Therefore, the total control law will become:

$$u_{sw} = -\hat{\mu}_s + K_s S + \hat{\rho} sat(S) \tag{46}$$

and

$$\frac{d}{dt}V = -K_s S^T S - \hat{\rho} S^T sat(S) \leq 0 \tag{47}$$

Since the time-derivative of Lyapunov function V is definitely negative, the proposed voltage control system is asymptotically stable. The above-mentioned procedure can be equally treated for eliminating the negative-sequence components of the k^{th} DG voltage busbar $(v_{dk}^{-,*} = 0, v_{qk}^{-,*} = 0)$ in normal operating conditions with unbalanced loads ($\bar{Z}_{li}$) or in abnormal conditions (faulted conditions) with either balanced or unbalanced loads. As a result, the (dq^e) k^{th} SV-PWM inverter voltages which command the k^{th} SV-PWM inverter can be obtained as:

$$v_{dqk}^{e,*} = (v_{dq}^{-})^{e,*} + (v_{dq}^{+})^{e,*} \tag{48}$$

Having the modeled SV-PWM inverter with reference voltages($v_{dqk}^{e,*}$), solving the inverter link state equations results in obtaining the inverter output currents which must be injected to MG positive- and negative-sequence networks. To this end, it is necessary to filter the DC transient components of I_d^e and I_q^e, resulting in the separation of positive and negative components defined by $I_{dq}^{e,+}$ and$I_{dq}^{e,-}$. As mentioned earlier, these currents are injected to the related MG network sequences for calculating the network positive and negative voltages which are to continue the step-by-step calculation procedure for the subsequent step time(Δt). Note that the injected currents at the first step come from the MG load flow solution in the steady-state normal operating condition. One more point is that, at each step time(Δt), the positive sequence injected by the slack or infinite bus must be obtained by solving the positive (Y) matrix equation of the network. This injection current is needed to obtain the MG positive network voltages used for the subsequent step time of calculation. Since the controller is designed in the synchronous reference frame, the sequence detection of system voltages and currents is also realized based on synchronous frame moving average filter (MAF) in the dq-frame [28]. The moving average filter acts as an ideal filter when the window's width is properly selected for the application [29-31]. Thus, in this paper, the sequence detection of system voltages and currents is realized based on MAF. To understand the MAF, the transfer function has been obtained and analyzed. Given an input signal

$$x(t) = Asin(\omega t + \theta_0) \tag{49}$$

with $\omega = 2\pi/T$, the output of the MAF will be:

$$\bar{x}(\mathrm{t}) = \frac{A}{\omega T_\omega}\{Cos[\omega(t - T_\omega) + \theta_0] - Cos(\omega t + \theta_0)\} \tag{50}$$

when using the MAF to filter dq components, if $T_\omega = \frac{T}{2}$, the dq even-order oscillations from odd-order harmonics and the negative sequence would be completely removed. If even-order harmonics with significant amplitudes are expected, the window width of the MAF should be increased to $T_\omega = T$ [28].

5. Simulation Results

In order to evaluate the effectiveness of the proposed control strategy and the presented fault analysis method, the MG study system demonstrated in Fig. 8 has been simulated in MATLAB. In addition, the performance of the proposed control strategy is compared with that of the PI-based active and reactive power controller and the SMC current controller, and the current references are obtained from [9]. In the studied system, all DG units are equipped with the same controller. DGs and loads use ungrounded isolation transformers (e.g. delta/un-grounded wye transformers, ungrounded wye/ungrounded wye transformers) to be connected to the MG.

The initial steady-state condition of MG is obtained by means of AC load flow analysis. In this paper, it is assumed that MG operates in the grid-connected mode. The system parameters are given in Table III. For any fault scenario occurring in the ungrounded MG system, the system nonlinear differential equations are solved by means of MATLAB code. The MG operates in the normal mode and DG1, DG2, DG3, and DG4 generate 700 kVA (0.07 p.u.), 1100kVA (0.11 p.u.), 900 kVA (0.09 p.u), and 500 kVA (0.05 p.u.), respectively, with 0.95 lagging power factor. Two types of load is considered in this simulation: balanced load and unbalanced load. The control parameters are listed in Table IV.

5.1. Single-line-to-ground fault

In this scenario, the ungrounded MG initially operates in the normal mode and all DGs generate rated active and reactive power. Then, a single-phase-to-ground fault occurs between phase (a) and ground in the middle of the transmission line between bus 6 and bus 9 at t=0.1 s (the fault can occur at any place in MG). The performance of the PI controller, SMC controller and adaptive SMC controller, under fault is demonstrated in this section.

5.1.1. PI-based active and reactive power controller

Fig. 9-(a-f) illustrates the system's response to the fault, while the DG1 employs a PI-based controller and the rest of DGs employ adaptive SMC controllers. A single-phase-to-ground fault occurs between phase (a) and ground in the middle of the transmission line between bus 6 and bus 9 at t=0.1 s, and then the fault is cleared at t=0.2 s. The output voltage, current and powers of the DG1 are shown in Fig.9 (a-c). Based on Fig 9. (a-b) the DG1 output voltage drops and the output current increases unsymmetrically during the fault. Besides, Fig, 9-c indicates that the DGs' output active and reactive powers are stable under normal condition, Nevertheless, the DG1 output powers are unstable during fault with the PI-based power controller, while other DGs with the adaptive SMC controller remain stable. It is observed that, under a fault condition, the controller parameters of the PI-controller need retuning and it is, therefore, not robust.

5.1.2. SMC current controller

In this section, all DGs employ the SMC-based current controller and the current references are obtained based on [9]. In this paper, with the tuning of k_p and k_q, the fault current amplitude is limited during the fault. A single-phase-to-ground fault occurs at t=0.1 s and then the fault is cleared at t=0.2 s. As shown in Fig. 10, when output active and reactive powers track their references, the fault current of DGs increases. Moreover, based on Fig. 11, with a limited-current fault, output active and reactive powers do not follow their reference values and the output voltage decreases in both cases. It is observed that, in contrast to the PI-based control, all of the controllers remain stable during fault and post-fault.

5.1.3. ASMC controller (proposed controller)

Fig. 12 illustrates the system's response to the single-phase-to-ground fault as those in previous cases but with the DGs employing the proposed adaptive SMC. The main aim of the proposed controller is to regulate output

active and reactive powers as well as the output voltage.

It is worth mentioning that, in this case, the DG voltages are almost sinusoidal and balanced during the fault since the negative-sequence voltages contribute to the creation of reactive power references.

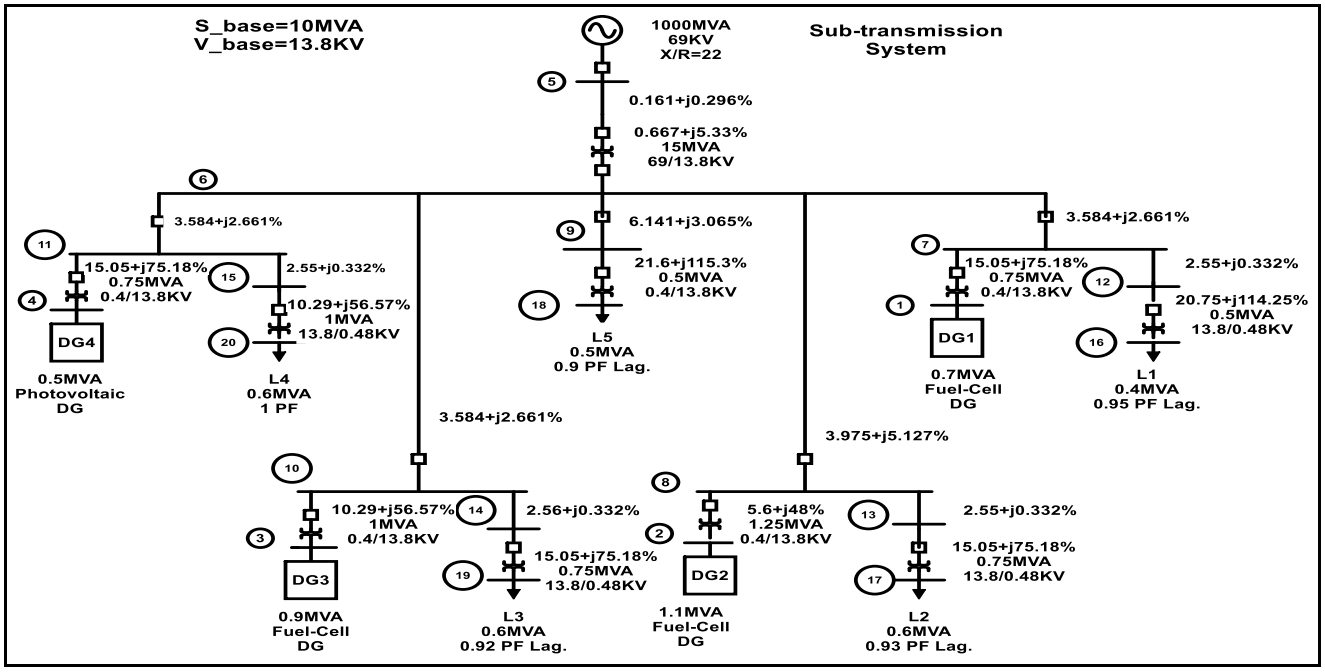

Fig. 8. Schematic diagram of the MG under consideration

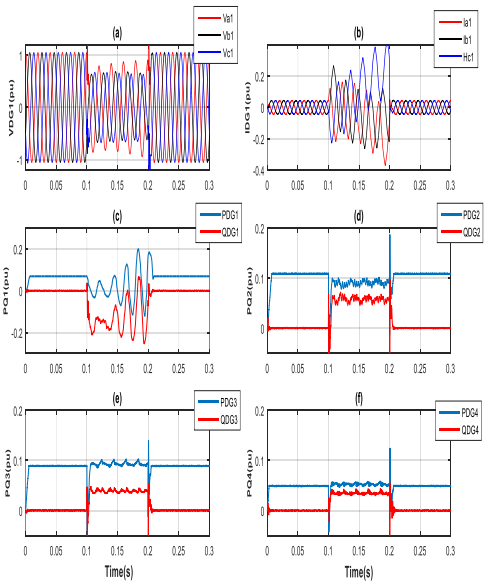

Fig. 9. System response with the PI-based power controller in DG1; a-b) The output voltage and current of DG1, c-f) the active and reactive power of DGs

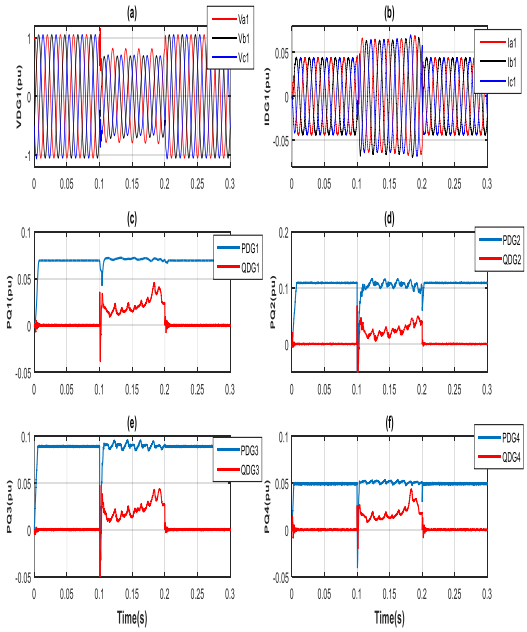

Fig. 10. System response with the SMC current controller in DGs ($k_p = -1$, $k_q = 1$); a-b) The output voltage and current of DG1, c-f) the active and reactive power of DGs

Considering these plots, it can be seen that the average values of the active and reactive power of DGs track their corresponding references, even under the single-phase-to-ground fault conditions. Since the adaptive SMC controller is designed for the positive and negative sequence of active and reactive powers, the negative sequences of the output voltage and current of DGs are eliminated and double-frequency oscillations do not appear. Consequently, the performance of the controller is desirable, although small distortions are observed in active and reactive powers.

5.2. Double-line Fault

Fig. 13 (a-b) illustrates the system's response to a double-line fault in which the DGs use the current controller. It is clear that the output voltage and current of DG1 are unbalanced and the voltage decreases and the current increases considerably. Fig. 13 (c-d) shows the output voltage and current of DG1 under the LL fault and ASMC controller. As expected, the negative component of voltage and current is properly eliminated by the ASMC controller, and the output voltage and current are balanced and limited. To evaluate the performance of the proposed controller, the output voltage and current of DG2 and the output power of all DGs under LL fault and unbalanced load are presented in Figs. 14 and 15. Fig. 14(a-f) indicates that the system's response under the LL fault is proper and the voltages and currents are balanced and limited. Fig. 15 (a-f) shows the system's response when a single phase inductive-resistive load is connected to phase (a) of bus 16 at t=0.1s (see table 3).

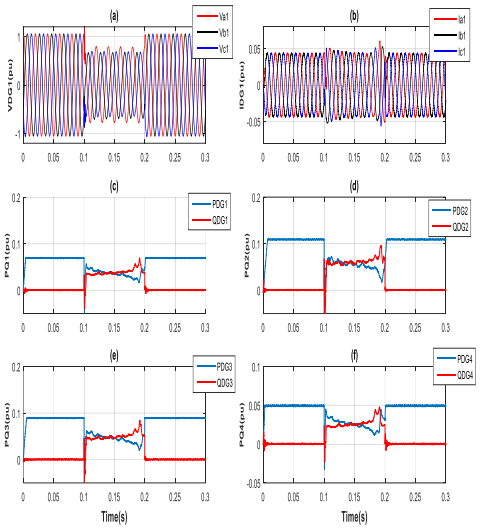

Fig. 11. System response with the SMC current controller in DGs ($k_p = -0.5$, $k_q = 0.5$); a-b) The output voltage and current of DG1, c-f) the active and reactive power of DGs

5.3. Power reference change for DG1

This scenario demonstrates the responses of the DG units to stepwise changes in their real power command and filters resistances and capacitors. To evaluate the robust performance of the proposed controllers subject to parametric uncertainties, a 50% mismatch is assumed for filters resistances and capacitors from $R_f = 0.012\Omega$ and $L_f = 5.2\,mH$ to $R_f = 0.5 \times 0.012\Omega$ and $L_f = 0.5 \times 5.2\,mH$ at $t = 0.4s$.

Moreover. At t = 0.1s active power reference of DG1, DG2 and DG3 are decreased to $P_{ref1} = 0.05pu$, $P_{ref2} = 0.0pu$, and $P_{ref3} = 0.0pu$. At t = 0.2s active power reference of DG1 set to zero and $P_{ref2} = 0.09pu$,

$P_{ref3} = 0.07pu$, $P_{ref4} = 0.00pu$. At t = 0.3s active power references of DGs are set to $P_{ref1} = 0.07$,$P_{ref2} = 0.11pu$, $P_{ref3} = 0.0pu$ and $P_{ref4} = 0.05pu$. At t = 0.4s active power reference of DG3 is set to $P_{ref3} = 0.09$. Fig. 16 depicts the system's response to the aforementioned sequence of events. It is observed that the output powers of DG units track their respective commands, thus resulting in corresponding variations in the real and reactive power outputs of the DG units.

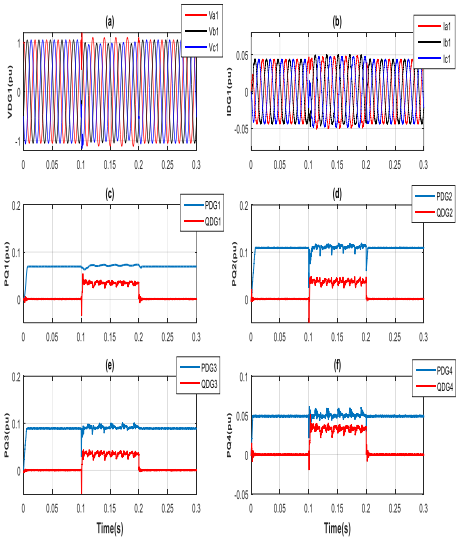

Fig. 12. System response with the proposed controller in DGs; a-b) The output voltage and current of DG1, c-f) the active and reactive power of DGs

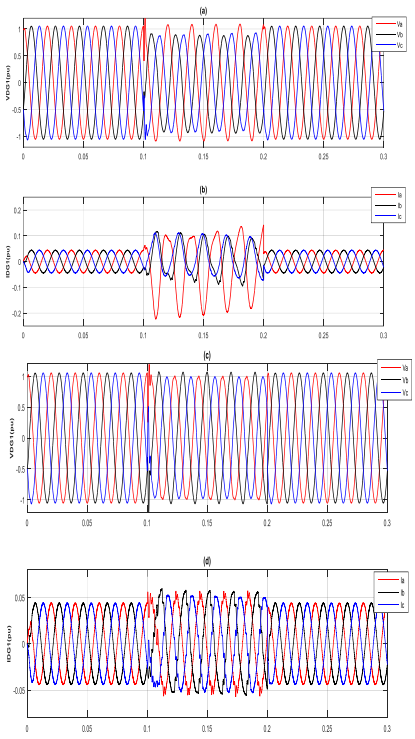

Fig. 13. The voltage and current of DG1. a-b) response of DG1 to the double-line fault with the current controller, c-d) response of DG1 to the double-line fault with the proposed controller.

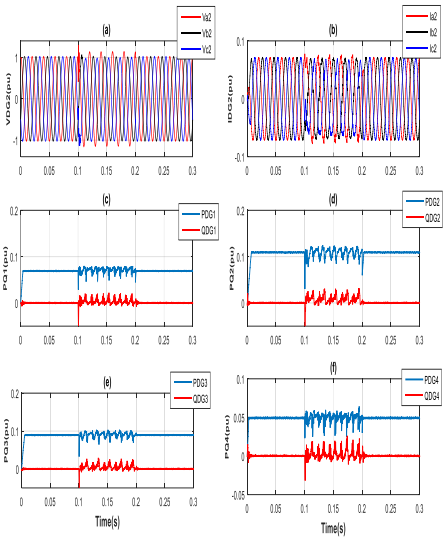

Fig. 14. Response of MG; a-b) The output voltage and current of DG2, c-f) the active and reactive power of DGs under the LL fault

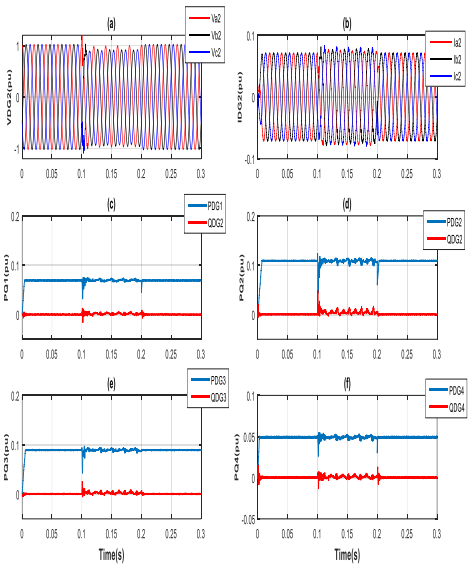

Fig. 15. Response of MG; a-b) The output voltage and current of DG2, c-f) the active and reactive power of DGs under unbalanced load

Table 3. System parameters

System parameters		
Grid voltage, line to line, rms Fundamental frequency	V_{s-rms} f_s	380 V 50 HZ
DC bus voltage	V_{dc}	675 v
Filter resistance	R_f	0.012Ω
Filter inductance	L_f	5.2mH
Filter capacitance	C_f	320μF
Switching frequency	f_{sw}	6480 Hz
Load resistance (single-phase)	R_L	0.3Ω
Load inductance(single-phase)	L_L	400mH

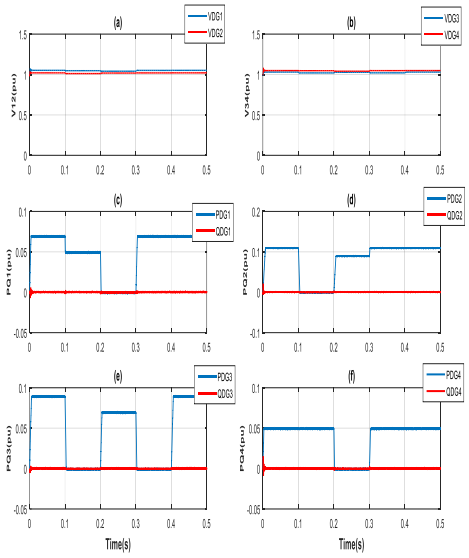

Fig.16 .System responses to the change in the reference power of DGs and 50% mismatch for filter resistances and inductors

Table 4. Controller parameters

Controller parameters	Symbol	values
Active power controller gain	K_{Ip}	8000
Reactive power controller gain	K_{IQ}	9500
Voltage controller gain	K_{IV}	1500
ASMC gain	K_S	10000
ASMC gain	K_ρ	1000
ASMC gain	ρ	1

6. CONCLUSION

This paper proposes an adaptive sliding mode controller for active and reactive regulation of DGs in a grid-connected MG containing several inverter-based DG units and unbalanced loads. The proposed control structure has two adaptive sliding mode-based active and reactive power controllers. The power controller ensures that the positive and negative sequences of active and reactive powers, generated by each DG unit, track its respective reference commands under both balanced and unbalanced conditions. Moreover, in this paper, a simple method has been described for the transient fault analysis of a grid-connected multi-DG MG. The proposed method is based on the quasi-stationary space phasors used in the studied MG. This method selects the combination of positive, negative and zero sequences of the MG network corresponding to any type of fault.

In the noted method, the dynamic model of DGs and quasi-stationary Y-matrix equations of the MG are solved with one-time step Δt of delay. Here, a Matlab code computer program has been developed, which is applicable to any size of the faulty MG for any type of fault. The results of the analysis allow for the design of a flexible active power controller capable of adapting itself to the fault situation and reconfigurable in case the grid requirements change. The performance of the proposed adaptive sliding mode controller (ASMC) is compared to that of a proportional-integral (PI)-based power controller and SMC current controller. Results show that the proposed controller properly regulates active and reactive powers while regulating the voltage of DGs Simulation results confirm the functionality and effectiveness of the fault study method proposed in this paper.

FUTURE RECOMMENDATION

In this work, we used a quasi-static model of the transmission network based on the assumption that phasors change slowly in comparison with system frequency ω_s. In recent years, with the increasing popularity of small distributed generators and fast power electronics-based devices, the assumption of quasi-static phasors cannot be accurate anymore. In order to describe the fast dynamic behavior and fast-amplitude and phase variations, our next work attempts to provide the dq0-based model of general transmission networks, which will be of low complexity and easy-to-use. Moreover, we can design an adaptive controller which regulates the voltages and current of all the buses of MG and loads.

REFERENCES

[1] N. Hatziargyriou, H. Asano, M.R. Iravani and C. Marnay. "Microgrids", *IEEE Power Energy Mag.*, vol. 5, no. 4, pp.78–94, 2007.

[2] S. N. Bhaskara and B. H. Chowdhury, "Microgrids-A review of modeling, control, protection, simulation and future potential," *Power Energy Soc. Gen. Meeting*, pp. 1-7, 2012.

[3] D.E. Olivares, A. Mehrizi-Sani, A.H. Etemadi, C.A Cañizares, R. Iravani, M. Kazerani, A.H. Hajimiragha, O. Gomis-Bellmunt, M. Saeedifard, R. Palma-Behnke and G.A. Jimenez-Estevez,"Trends in microgrid control", *IEEE Trans. Smart Grid*, vol. 5, no. 4, pp. 1905-1919. 2014.

[4] M. Allahnoori, S.H Kazemi, H. Abdi and R. Keyhani, "Reliability assessment of distribution systems in presence of microgrids considering uncertainty in generation and load demand", *J. Oper. Autom. Power Eng.*, vol. 2, no. 2, pp. 113- 120, 2014.

[5] H. Shayeghi and E. Shahryari, "Optimal operation management of grid-connected microgrid using multi objective group search optimization algorithm", *J. Oper. Autom. Power Eng.*, vol. 5, no. 2, pp. 227-239, 2017.

[6] P. Rodriguez, A.V. Timbus, R. Teodorescu, M. Liserre, and F. Blaabjerg, "Flexible active power control of distributed power generation systems during grid faults", *IEEE Trans. Ind. Electron.*, vol. 54, no. 5, pp. 2583 - 2592. 2007.

[7] A. Camacho, M. Castilla, J. Miret, J. C. Vasquez, and E. Alarcón-Gallo, "Flexible voltage support control for three-phase distributed generation inverters under grid fault", *IEEE Trans. Ind. Electron.*, vol. 60, no. 4, pp. 1429-1441, 2013.

[8] X. Guo, W. Liu and X. Zhang, "Flexible control strategy for grid-connected inverter under unbalanced grid faults without PLL," *IEEE Trans. Power Electron*, vol. 30, no. 4, pp. 1773-1778, 2015.

[9] X. Guo, W. Liu, Z. Lu and M. J. Guerrero "Flexible Power Regulation and Current-limited Control of Grid-connected Inverter under Unbalanced Grid Voltage Faults", *IEEE Trans. Ind. Electron.*, vol. 64, no. 9, pp. 7425-7432. 2017.

[10] S. Gholami. M. Aldeen, and S. Saha, "Control strategy for dispatchable distributed energy resources in islanded microgrids", *IEEE Trans. Power Syst*., vol. 33, no. 1, pp. 141-152, 2018.

[11] B. Vaseghi , M. A. Pourmina and S. Mobayen, "Secure communication in wireless sensor networks based on chaos synchronization using adaptive sliding mode control", *Nonlinear Dyn.*, vol. 89, no. 3, pp. 1689-1704, 2017.

[12] O. Mofid and S. Mobayen, "Adaptive sliding mode control for finite-time stability of quad-rotor UAVs with parametric uncertainties", *ISA Trans.*, vol. 72, pp. 1-14, 2018.

[13] S. Mobayen, "Design of novel adaptive sliding mode controller for perturbed Chameleon hidden chaotic flow", *Nonlinear Dyn.*, vol. 92, No. 4, pp. 1539-1553. 2018.

[14] Z. Chen, A. Luo and H. Wang ," Adaptive sliding-mode voltage control for inverter operating in islanded mode in microgrid", *Int. J. Electr. Power Energy Syst.*, vol. 66, pp. 133-143, 2015.

[15] M. B. Delghavi, S. Shoja-Majidabad and A. Yazdani, "Fractional-order sliding-mode control of islanded distributed energy resource systems", *IEEE Trans. Sustain. Energy*, vol. 7, no. 4, pp. 1482-1491, October 2016.

[16] M. B. Delghavi and A. Yazdani, "Sliding-mode control of ac voltages and currents of dispatchable distributed energy resources in master-slave-organized inverter-based microgrids", *IEEE Trans. Smart Grid*, 2017, DOI: 10.1109/TSG.2017.2756935

[17] S. K. Gudey and R. Gupta," Recursive fast terminal sliding mode control in voltage source inverter for a low-voltage microgrid system", *IET Gener., Trans. Distrib.*, vol. 10, no. 7, pp. 1536-1543, 2016.

[18] M. M.Rezaei and J. Soltani, "A robust control strategy for a grid-connected multi-bus microgrid under unbalanced load conditions", *Electr. Power Energy Syst.*, vol. 71, pp. 68–76, 2015.

[19] J. Mahseredjian, S. Lefebvre and X.D. Do, "A new method for time-domain modeling of nonlinear circuits in large linear networks", Proc. 11th *Power Syst. Comput. Conf.*, No. 4, 1993, pp. 915-922.

[20] S. Saha and M. Aldeen, "Dynamic modeling of power systems experiencing faults in transmission /distribution networks" *IEEE Trans. Power Syst.*, vol. 30, pp. 2349-2363, 2015.

[21] A. Coronado-Mendoza and A. Domínguez-Navarro, "Dyn-amic phasors modeling of inverter fed induction generator", *Electric Power Syst. Res.*, vol. 107 pp. 68-76. 2014.

[22] T.H. Demiray, "Simulation of power system dynamics using dynamic phasor models," *Swiss Federal Institute Technol.*, Zurich, 2008.

[23] S. Huang, R. Song, and X. Zhou, "Analysis of balanced and unbalanced faults in power systems using dynamic phasors", Proce. *Conf.* Power Syst. Thechnol., 2002.

[24] J. Belikov and Y. Levron, "Comparison of time-varying phasor and dq0 dynamic models for large transmission networks", *Electr. Power Energy Syst*., vol. 93 pp. 65-74, 2017

[25] D. Baimel, J. Belikov, J. M. Guerrero, and Y. Levron, "Dynamic modeling of networks, microgrids, and renewable sources in the dq0 reference frame: A survey," *IEEE Trans.*, vol. 5, pp. 21323-21335, 2017.

[26] J. J. Grainger and W. D. Stevenson, "Power system analysis," McGraw-Hill, Dey 11, 1372 AP, *Technol. Eng*. - 787 pages.

[27] J.E. Slotine, W. Li, "Applied nonlinear control," *Englewood Cliffs, NJ: Prentice-Hall*; 1991.

[28] E. Robles, S. Ceballos, J. Pou, J. Luis Mart, J. Zaragoza, and P. Ibanez, "Variable-frequency grid-sequence detector based on a quasi-ideal low-pass filter stage and a phase-locked loop", *IEEE Trans. Power Electron.*, vol. 25, no. 10, pp. 2552-2563, 2010.

[29] J. Pou, E. Robles, S. Ceballos, J. Zaragoza, A. Arias, and P. Ibanez, "Control of back-to-back-connected neutral-point-clamped converters in wind mill applications," presented EPE2007, Dresden, Denmark, Sep. 2-5.

[30] A. Ghoshal and V. John, "A Method to Improve PLL performance under abnormal grid conditions," presented at the NPEC2007, *Indian Inst. Sci., Bangalore, India*, Dec. 17-19.

[31] F. D. Freijedo, J. Doval-Gandoy, O. Lopez, and E. Acha, "A generic open loop algorithm for three-phase grid voltage/current synchronization with particular reference to phase, frequency, and amplitude estimation," *IEEE Trans. Power Electron.*, vol. 24, no. 1, pp. 94-107, Jan. 2009.